

## Electron scattering off the ground-state band and the $\gamma$ band in $^{150}\text{Nd}$

R. K. J. Sandor,<sup>(1)</sup> H. P. Blok,<sup>(1)</sup> U. Garg,<sup>(1,4)</sup> M. Girod,<sup>(2)</sup> M. N. Harakeh,<sup>(1)</sup> C. W. de Jager,<sup>(3)</sup>  
and H. de Vries<sup>(3)</sup>

<sup>(1)</sup>*Faculteit Natuurkunde en Sterrenkunde, Vrije Universiteit, de Boelelaan 1081, 1081HV Amsterdam, The Netherlands*

<sup>(2)</sup>*Service de Physique et Techniques Nucléaires, Commissariat à l'Energie Atomique, Bruyères-le-Châtel,  
Boîte Postale 12, F-91680 Bruyères-le-Châtel, France*

<sup>(3)</sup>*Nationaal Instituut voor Kernfysica en Hoge-Energiefysica, sectie K (NIKHEF-K),  
P. O. Box 4395, 1009AJ Amsterdam, The Netherlands*

<sup>(4)</sup>*Physics Department, University of Notre Dame, Notre Dame, Indiana 46556*

(Received 14 September 1990)

Inelastic electron scattering to levels of the ground-state band and the  $\gamma$  band in  $^{150}\text{Nd}$  was studied in a momentum transfer range of 0.5–2.8  $\text{fm}^{-1}$ . The extracted transition charge densities were compared to microscopic Hartree-Fock-Bogoliubov calculations. The overall agreement between the data and the calculations is good, indicating that the dynamic properties of the rotational collective degrees of freedom in statically deformed nuclei can be well described in this microscopic model.

The nucleus  $^{150}\text{Nd}$ , with its well-developed rotational bands, is an excellent testing ground for a microscopic description of low-lying collective transitions in deformed nuclei. Nuclear charge and current densities provide information about the dynamic properties of the various excitation modes and hence will reflect differences between various collective excitations. Because of the well-understood relationship between the measured cross section in electron scattering and these densities, electron scattering is the designated tool to investigate the spatial properties of the nuclear wave function. Although much effort has already been spent in the investigation of the ground-state bands of deformed nuclei, such as  $^{152}\text{Sm}$ ,<sup>1</sup>  $^{154}\text{Gd}$ ,<sup>2</sup> and also  $^{150}\text{Nd}$ ,<sup>3</sup> until now very little data for the  $\gamma$  band<sup>2</sup> have been published in this mass region. The reason for this is the high level density in deformed nuclei even at moderately low excitation energies, which makes it difficult to resolve states belonging to different bands. As a consequence of the high resolution obtained in the present experiment it was possible to extract transition densities for the quadrupole and the hexadecapole states of the  $\gamma$  band in  $^{150}\text{Nd}$ . In this Rapid Communication these data and those for the  $2^+$ ,  $4^+$ , and  $6^+$  states of the ground-state band are presented. The data are compared with results of a microscopic mean-field theory that describes  $^{150}\text{Nd}$  taking into account triaxial deformations. The potentials, collective masses, and moments of inertia used in the Bohr Hamiltonian were calculated in the framework of the Hartree-Fock-Bogoliubov (HFB) method with a density-dependent force without any free parameters. For more elaborate information on such calculations, the reader is referred to Refs. 1, 4, and 5.

The data were taken at the NIKHEF-K facility<sup>6</sup> with the magnetic quadrupole-dipole-dipole (QDD) spectrometer. In order to be able to resolve the different states at excitation energies up to 2 MeV the best possible resolution was needed. By means of software corrections (ray-tracing algorithms)<sup>7</sup> we were able to obtain an energy resolution between 12 keV for the lowest incident electron

energy (112 MeV) up to 30 keV for the highest (450 MeV). The scattering angles ranged from  $36^\circ$  to  $83^\circ$ , corresponding to effective momentum transfers  $q_{\text{eff}} = q[1 + 1.33(Z\hbar c/EA)^{1/3}]$  between 0.5 and 2.8  $\text{fm}^{-1}$ . This  $q$  range is large enough to permit the determination of the ground-state charge density or the transition charge densities for many levels of interest. One additional measurement at a backward angle of  $154^\circ$  and an energy of 80 MeV was performed to investigate possible transverse contributions to the form factors.

The spectrometer acceptance solid angle was varied between 0.35 and 5.6 msr. The overall efficiency of the event trigger system was checked before each measurement by a short run on the elastic and inelastic scattering to the first excited state of  $^{12}\text{C}$ , and was always found to be larger than 98%. The collected charge was measured with a toroid monitor with an accuracy of 0.1%. The target was a foil of 95% isotopically enriched  $^{150}\text{Nd}$  with a nominal thickness of 10  $\text{mg}/\text{cm}^2$ . For optimum resolution the target was set in transmission mode. Most of the data were taken in an event-by-event mode, to allow off-line software corrections for kinematical broadening and spectrometer aberrations. For the smallest  $q$  values this was not possible due to the high count rates and therefore data were acquired on-line in spectral form. However, since these low- $q$  measurements were made at forward angles with a small solid angle of 0.35 msr, the loss in resolution due to the kinematical broadening and spectrometer aberrations was negligible.

Cross sections were extracted from the measured spectra by a line-shape fitting technique with the program ALLFIT.<sup>8</sup> Uncertainties due to detector efficiencies, target alignment, and solid angle were corrected for by the aforementioned efficiency calibration runs on  $^{12}\text{C}$ . These runs were combined with a run on a natural boron-nitride target and the runs on other Nd isotopes to provide the energy calibration with the usual method of recoil energy differences. The only remaining unknown factor was the uniformity of the target; its average contribution over the

beam spot area to the experimental uncertainty was estimated to be less than 1%.

The distorted-wave Born approximation (DWBA) code FOUBES (Ref. 9) was employed to extract the transition charge densities. These densities were parametrized using the Fourier-Bessel series:

$$\rho_\lambda(r) = \sum_{\mu} A_{\mu} q_{\mu}^{(\lambda-1)} j_{\lambda}(q_{\mu}^{(\lambda-1)} r), \quad r < R_c, \quad (1)$$

$$\rho_\lambda(r) = 0, \quad r > R_c,$$

where  $q_{\mu}^{(\lambda-1)} R_c$  is the  $\mu$ th zero of the spherical Bessel function  $j_{\lambda-1}(x)$  and  $R_c$  is a cutoff radius, beyond which  $\rho_\lambda(r)$  is so small that it can be neglected. The transition current  $J_{\lambda,\lambda+1}$  was neglected in the analysis, which seems a reasonable assumption in the light of the relatively forward scattering angle, which never exceeded  $83^\circ$ , and the expected small contribution of the transverse form factor to such collective transitions. This assumption is confirmed by the analysis of the backward angle data point at 80 MeV, where the transverse components of the cross section for the investigated states turned out to be less than 3% of the longitudinal ones. In order to eliminate unphysical oscillations in the transition charge densities at large radii, a so-called tail bias<sup>10</sup> was applied. Furthermore, to account for the form factor behavior beyond the maximum transverse momentum measured, a high- $q$  constraint was used to determine the incompleteness error. For the first and third  $2^+$  states values for the reduced transition probability  $B(E2)$ , as known from the literature,<sup>11</sup> were added as data points. The relation between  $B(E\lambda)$  and the transition charge density for a transition

from a  $0^+$  state to a natural parity state with spin  $\lambda$  is

$$B(E\lambda) = (2\lambda + 1) \left| \int_0^\infty \rho_\lambda(r) r^{2+\lambda} dr \right|^2. \quad (2)$$

This quantity basically determines the form factor at the photon point.

The resulting transition charge densities for the  $2_1^+$ ,  $4_1^+$ , and the  $6_1^+$  states are shown in Fig. 1 together with those of the  $2_3^+$  and  $4_3^+$  states. As can be seen from the figure, the overall structure of the transition charge densities for the  $2_1^+$  and  $2_3^+$  states are very similar to each other. The same is true for the  $4_1^+$  and  $4_3^+$  states. However, the radius where the transition charge densities peak is shifted by the same amount to a lower value in the case of the  $2_3^+$  and  $4_3^+$  states compared to the  $2_1^+$  and  $4_1^+$  states, respectively. This shift can be attributed to the fact that the  $2_3^+$  and  $4_3^+$  states are known to be members of the  $\gamma$  band,<sup>12</sup> which constitutes a vibration along the short axis superposed on a static deformation. This means that the overlap of the wave functions of the initial state and the final state will peak at a smaller radius than the same overlap in the case of excitations of the ground-state band, which peaks in first order at the average nuclear radius.

The calculations that have been performed make use of a mean-field theory. The intrinsic and collective aspects of nuclear motion are taken into account in a self-consistent way. In this approach, first an effective nuclear Hamiltonian is assumed which describes the nucleus as an assembly of independent quasiparticles moving in a mean field generated by all nucleons. The ground state of this system is calculated by solving the self-consistent Hartree-Fock-Bogoliubov (HFB) equations. Here a constrained HFB method is used allowing an intrinsic defor-

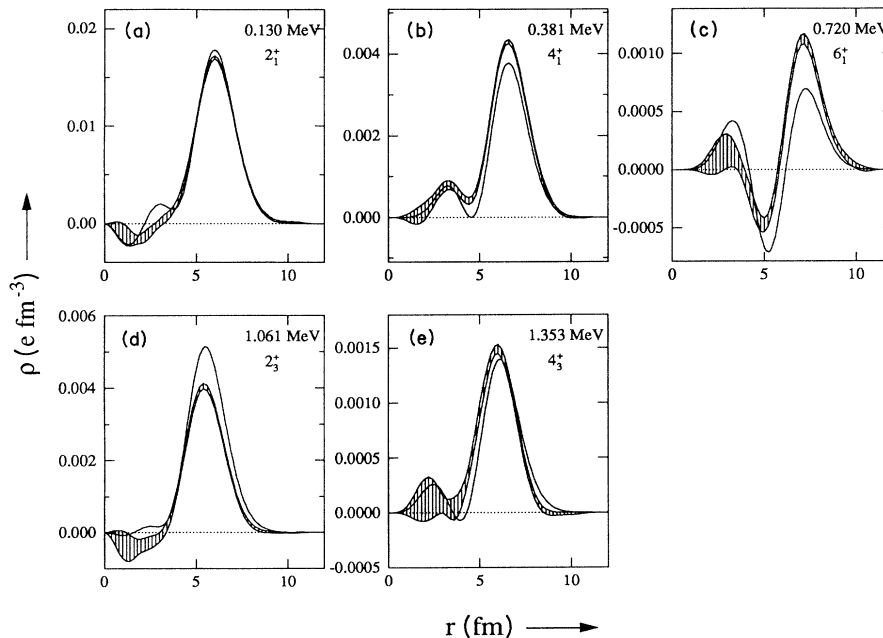


FIG. 1. Transition densities of the ground-state band and the  $\gamma$  band of  $^{150}\text{Nd}$  as obtained from experiment (curves with error band) are compared to results of microscopic calculations (solid line). The (a)  $2_1^+$  state, the (b)  $4_1^+$  state, the (c)  $6_1^+$  state, the (d)  $2_3^+$  state, and the (e)  $4_3^+$  state are shown. The error bands include the statistical errors as well as the model or incompleteness error.

mation to be ascribed to a rearrangement of the average and the pairing fields. The constraints were imposed by means of the  $q_{20}$  and  $q_{22}$  (or  $\beta$  and  $\gamma$ ) variables.<sup>1</sup> The reason these constraints were used is that the first  $2^+$  and  $4^+$  levels are very collective levels corresponding to quadrupole deformations. Therefore, the HFB calculations permit not only to calculate the deformation in the minimum of the potential energy surface (PES), but also to maintain the more or less large rigidity of the nucleus with respect to quadrupole deformations. The force used in the calculations is the *D1S* force, a variation of the well known *D1* force<sup>13</sup> with improved surface properties.<sup>1</sup> In the calculation of the PES eleven major shells were used.

Figure 2 shows the PES of <sup>150</sup>Nd. The static minimum is located near  $\beta=0.3$  and  $\gamma=0^\circ$ , which gives a pure prolate deformation. The cuts in the PES plane along the  $\gamma=0^\circ$  and  $\gamma=60^\circ$  lines are typical for well-deformed nuclei. Although the barrier for a spherical form of the nucleus is relatively high along  $\gamma=0^\circ$ , the minimum in the PES is rather soft in the direction of increasing  $\gamma$  for  $\beta < 0.3$ . This shallowness of the minimum indicates that <sup>150</sup>Nd cannot be described with only the HFB wave function corresponding to the minimum in the potential energy, i.e., a single Slater determinant.

Therefore, a dynamical treatment is necessary to determine the dynamical deformation of both the ground state and excited states. To this end a Bohr-like Hamiltonian<sup>14</sup> was used in the following form:

$$H = V(\beta_0, \beta_2) + \frac{1}{2} \left( B_{00}\beta_0^2 + 2B_{02}\beta_0\beta_2 + B_{22}\beta_2^2 + \sum_i \frac{J_i^2}{I_i} \right). \quad (3)$$

Here the collective variables  $\beta_0$  and  $\beta_2$  are related to the Bohr parameters  $\beta$  and  $\gamma$  by  $\beta_0 = \beta \cos(\gamma)$  and  $\beta_2 = \beta \sin(\gamma)$ . This Hamiltonian is the Gaussian overlap approximation of the Hill-Griffin-Wheeler equation. It is

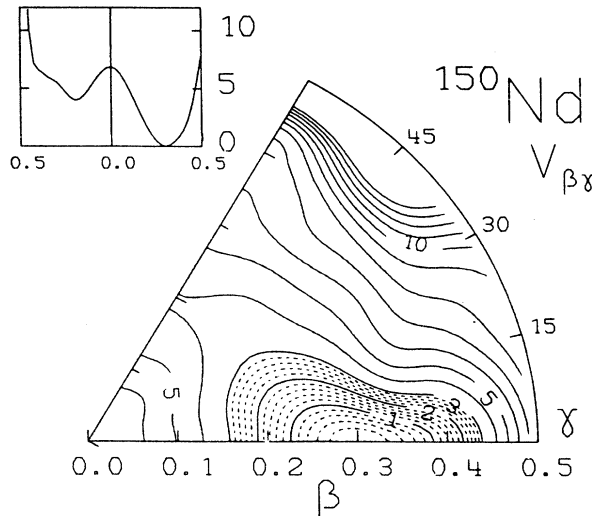


FIG. 2. Contour plot of the calculated potential-energy surface of <sup>150</sup>Nd. The inset represents cuts in the PES along  $\gamma=0^\circ$  and  $\gamma=60^\circ$ .

diagonalized including the PES as collective potential and using the inertia parameters which were calculated in the cranking approximation<sup>15</sup> starting from the HFB quasi-particle wave functions.

Figure 3 shows the collective wave function for the ground state. The maximum of this  $0_1^+$  wave function is located at a smaller  $\beta$  deformation than the minimum of the PES. The dynamical  $\gamma$  deformation is  $\gamma=15^\circ$ , to be compared to  $\gamma=0^\circ$  for static deformation. This shift from a prolate shape to a triaxial shape confirms the necessity to perform these calculations in a dynamical framework.

At this point transition densities for transitions between the ground state and excited states can be calculated. Specializing to even-even rotational nuclei, the transition density can be written as

$$\rho_{tr} = \langle 0 | \rho | I \rangle = \sum_{K=0}^I \int A_{00}(q_0, q_2) A_{IK}(q_0, q_2) \times Q_{IK}^{q_0, q_2}(r) dq_0 dq_2, \quad (4)$$

with  $A_{IK}$  being the collective wave function coming from the Bohr Hamiltonian diagonalization and with

$$Q_{IK}^{q_0, q_2}(r) = \frac{1}{(4\pi)^{1/2}} \int \rho_{q_0, q_2}(r) \left( \frac{Y_{IK}^*(\Omega) + (-)^K Y_{IK}^*(\Omega)}{[2(1 + \delta_{K0})]^{1/2}} \right) d\Omega. \quad (5)$$

Here  $\rho_{q_0, q_2}(r)$  is the spatial HFB charge density folded with the finite size of the nucleons and corrected for center-of-mass effects. The variables  $q_0$  and  $q_2$  refer to the  $q_{20}$  and  $q_{22}$  variables mentioned earlier, respectively.

To calculate the transition charge densities two approximations were invoked.<sup>1</sup> First, a sharp angular overlap between the HFB wave functions was assumed. This has

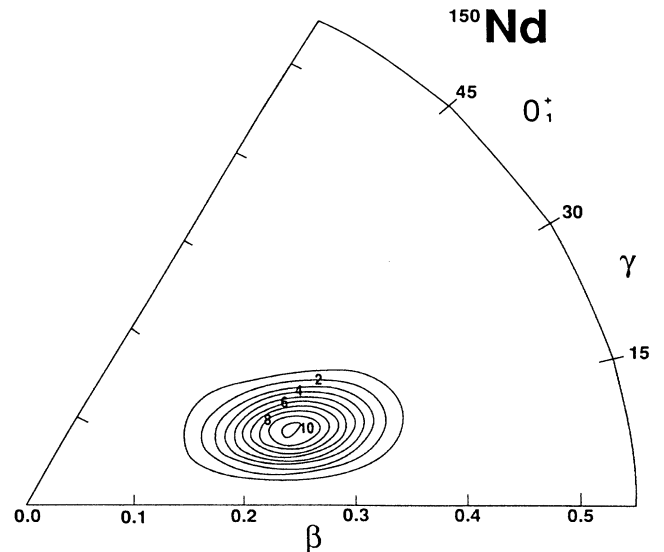


FIG. 3. Contour plot of the ground-state wave function of <sup>150</sup>Nd as obtained from the fully dynamical calculation.

been justified for well-deformed nuclei.<sup>16</sup> Second, the overlap of the wave function of the ground state and the wave function of the excited state is also assumed to be sharp.

In Fig. 1 the results of the theoretical calculations are compared with the experimental transition densities. As can be seen, the overall agreement is good. Both the strength and the structure of the transition charge densities of the  $2_1^+$  and  $4_3^+$  states are very well reproduced, whereas the agreement for the other states is not as good. For the ground-state band of  $^{152}\text{Sm}$  similar good agreement between experiment and calculations was obtained.<sup>1</sup> We emphasize that no parameter of the nucleon-nucleon interaction or of the PES has been adjusted to optimize agreement with the experiment.

A closer look reveals that in general the quadrupole states are slightly overestimated whereas the hexadecapole states are slightly underestimated. Although the shift of the transition charge densities inward in case of the  $\gamma$  band is reproduced, the calculated shift is slightly less than seen in the experiment. Moreover, the calculated ratio of the transition charge densities of the  $\gamma$  band with respect to the ground-state band is larger than seen in the experiment, leading to a somewhat larger discrepancy for the  $2_3^+$  state. The fact that both  $4^+$  transition charge densities peak more outward than those of the  $2^+$  states is an evidence of a positive hexadecapole moment for  $^{150}\text{Nd}$ . This confirms the results of previous theoretical calculations by Götz *et al.*<sup>17</sup>

The agreement for the  $6_1^+$  state of the ground-state band is not as good as for the other states. To investigate this deviation between theory and experiment, calculations along the lines of the Davydov-Filippov formalism<sup>18</sup> were performed. These calculations single out values of  $\beta$  and  $\gamma$  in the PES plane, which are subsequently used to calculate the corresponding transition charge density. Thus an indication is obtained as to what the possible reason for the discrepancies between the calculations and the experiment may be. The results of these static calculations are shown in Fig. 4 together with the experimental transition charge density of the  $6_1^+$  state. It turns out that a larger value of  $\beta$  and/or  $\gamma$  than found in the dynamic calculation leads to a better agreement with the data. This indicates that the PES as determined in the HFB treatment is possibly not soft enough in the direction of increasing  $\beta$  or  $\gamma$  deformation. To draw final conclusions on this point, however, is premature before the influence of these larger values for  $\beta$  and  $\gamma$  on the other states presented is investigated. Such an investigation will be performed and the results will be published in a future, more extensive paper on  $^{150}\text{Nd}$ .

In conclusion, the results of an electron-scattering experiment on  $^{150}\text{Nd}$  have been presented. Transition charge densities of the  $2_1^+$ ,  $4_1^+$ , and  $6_1^+$  states have been obtained, together with those of the  $2_3^+$  and  $4_3^+$  states, which are confirmed as members of the  $\gamma$  band. The tran-

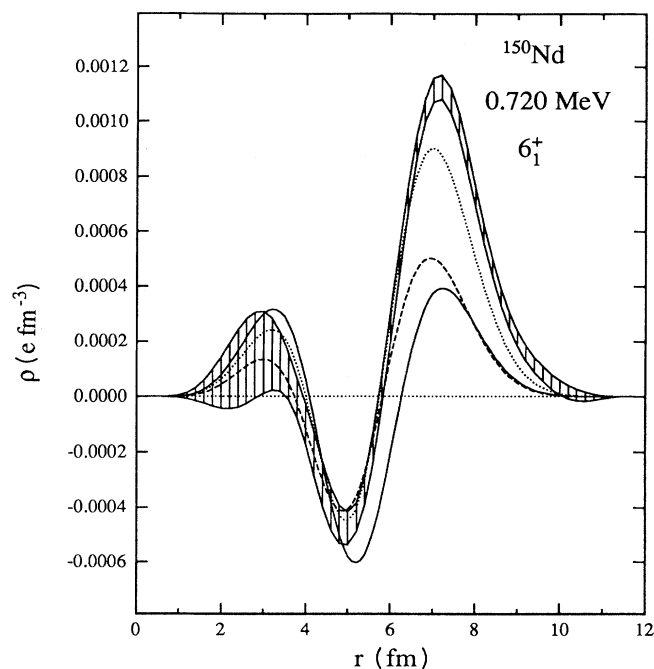


FIG. 4. The results from the static Davydov-Filippov calculations are compared to the experimental transition density of the  $6_1^+$  state of  $^{150}\text{Nd}$  (curve with error band). The different curves represent different positions in the  $\beta\gamma$  plane: solid,  $\beta=0.27, \gamma=20^\circ$ ; dashed,  $\beta=0.27, \gamma=30^\circ$ ; dotted,  $\beta=0.34, \gamma=30^\circ$ .

sition charge densities are compared to theoretical calculations in a dynamical, triaxial HFB framework, where no parameters were adjusted. The potential energy surface is that of a prolate deformed nucleus, the minimum lying at  $\beta=0.3$  and  $\gamma=0^\circ$ . To describe the transition charge densities a fully dynamical calculation has been performed, thus accounting for the softness of the minimum in the direction of increasing  $\gamma$ . The calculations reproduce both the shift inward of transition densities of the states of the  $\gamma$  band and the positive hexadecapole moment of the nucleus, but more importantly, the overall agreement between the calculated transition densities and the data is good. The deviation observed for the transition density of the  $6^+$  state of the ground-state band from the calculated one can possibly be ascribed by means of Davydov-Filippov calculations to a larger softness in the  $\beta$  and  $\gamma$  direction than predicted.

Two of the authors (U.G. and M.G.) wish to acknowledge the hospitality of the experimental nuclear physics group at the Vrije Universiteit. This work is part of the research program of the Foundation for Fundamental Research of Matter (FOM), which is financially supported by the Netherlands' Organization for Scientific Research (NWO).

- <sup>1</sup>X. H. Phan *et al.*, *Phys. Rev. C* **38**, 1173 (1988).  
<sup>2</sup>F. W. Hersman *et al.*, *Phys. Rev. C* **33**, 1905 (1986).  
<sup>3</sup>A. S. Hirsch, Ph.D. thesis, MIT, 1977 (unpublished).  
<sup>4</sup>H. Flocard, P. Quentin, A. A. Kerman, and D. Vautherin, *Nucl. Phys. A* **203**, 433 (1973).  
<sup>5</sup>M. Girod and B. Grammaticos, *Phys. Rev. C* **27**, 2317 (1983).  
<sup>6</sup>C. de Vries *et al.*, *Nucl. Instrum. Methods* **223**, 1 (1984).  
<sup>7</sup>H. Blok, E. A. J. M. Offerman, C. W. de Jager, and H. de Vries, *Nucl. Instrum. Methods Phys. Res. Sect. A* **262**, 29 (1987).  
<sup>8</sup>C. E. Hyde-Wright, Ph.D. thesis, MIT, 1984 (unpublished).  
<sup>9</sup>J. H. Heisenberg and H. P. Blok, *Annu. Rev. Nucl. Part. Sci.* **33**, 569 (1983).  
<sup>10</sup>J. H. Heisenberg, *Adv. Nucl. Phys.* **12**, 61 (1981).  
<sup>11</sup>S. W. Yates, N. R. Johnson, L. L. Reidinger, and A. C. Kahler, *Phys. Rev. C* **17**, 634 (1978).  
<sup>12</sup>M. Sakai, *At. Data Nucl. Data Tables* **31**, 399 (1984).  
<sup>13</sup>J. Decharge and D. Gogny, *Phys. Rev. C* **21**, 1568 (1980).  
<sup>14</sup>K. Kumar, in *The Electromagnetic Interaction in Nuclear Physics*, edited by W. D. Haminton (North-Holland, Amsterdam, 1975).  
<sup>15</sup>D. R. Inglis, *Phys. Rev.* **103**, 1786 (1956).  
<sup>16</sup>A. Zaringhalam and J. W. Negele, *Nucl. Phys. A* **288**, 417 (1977).  
<sup>17</sup>U. Götz, H. C. Pauli, K. Adler, and K. Junker, *Nucl. Phys. A* **192**, 1 (1972).  
<sup>18</sup>A. S. Davydov and G. F. Filippov, *Nucl. Phys.* **8**, 237 (1958).